AN ENHANCED DIRECTIONAL TOTAL GENERALIZED VARIATION MODEL FOR SPECKLE NOISE REMOVAL IN DIGITAL IMAGES

MÔ HÌNH BIẾN PHÂN TỔNG QUÁT CÓ HƯỚNG CẢI TIẾN ĐỂ KHỬ NHIỄU ĐỐM TRÊN ẢNH SỐ

Pham Cong Thang*, Truong Tan Cuong, Nguyen Nguyen Anh, Nguyen Thanh Than

The University of Danang - University of Science and Technology, Vietnam

*Corresponding author: pcthang@dut.udn.vn

(Received: March 27, 2025; Revised: April 29, 2025; Accepted: May 12, 2025)

DOI: 10.31130/ud-jst.2025.162

Abstract - Speckle noise is one of the most common types of noise, degrading image quality and affecting analytical and predictive applications. Various methods have been proposed for speckle noise removal in digital images. However, these methods still have limitations, such as loss of important details, edge blurring, or failure to preserve crucial image structures. In this paper, we propose a novel model, DTGV-g, which combines Directional high-order Total Generalized Variation with an edge detection method to enhance image quality after denoising. This approach not only effectively removes noise but also preserves edges and essential image structures. The Chambolle-Pock algorithm is employed to solve the optimization problem. Experimental results demonstrate that the proposed DTGV-g model achieves superior performance compared to other methods. Notably, our approach remains effective even in cases where the image is blurred or has a high level of noise.

Key words - Image denoising; speckle noise; edge detection; total variation; directional total generalized variation

Tóm tắt - Nhiễu đốm (speckle noise) là một trong những loại nhiễu phổ biến, làm xuống cấp chất lượng hình ảnh và ảnh hưởng đến các ứng dụng phân tích và dự đoán. Để khử nhiễu đốm trên ảnh số, nhiều phương pháp đã được đề xuất. Tuy nhiên, chúng vẫn gặp phải những hạn chế như mất chi tiết quan trọng, làm mờ biên hoặc không bảo toàn được các kết cấu quan trọng trong ảnh. Trong bài báo này, một mô hình mới DTGV-g, kết hợp biến phân tổng quát bậc cao có hướng với phương pháp phát hiện biên nhằm nâng cao chất lượng ảnh sau khử nhiễu, được đề xuất. Cách tiếp cận này không chỉ loại bỏ nhiễu hiệu quả mà còn bảo toàn được biên và các kết cấu quan trọng của hình ảnh. Thuật toán Chambolle-Pock được sử dụng để giải bài toán tối ưu. Kết quả thực nghiệm cho thấy, mô hình DTGV-g đề xuất đạt hiệu suất vượt trội so với các phương pháp khác. Đặc biệt, phương pháp của chúng tôi vẫn hoạt động tốt ngay cả khi ảnh bị làm mờ hoặc có mức độ nhiễu cao.

Từ khóa - Khử nhiễu ảnh; nhiễu đốm; phát hiện biên; biến phân tổng; biến phân tổng quát có hướng

1. Introduction

The use of digital images has become increasingly essential across various engineering and scientific fields. In medicine, ultrasound images are frequently affected by speckle noise, which obscures small anatomical structures and complicates accurate diagnosis. In aerospace and remote sensing, Synthetic Aperture Radar (SAR) images - an important data source for monitoring the Earth's surface - are often degraded by speckle noise, reducing object recognition and terrain analysis capabilities. Improving image quality through effective speckle noise reduction techniques is therefore of paramount importance, directly contributing to enhanced accuracy in analysis, prediction, and decision-making in these domains. Generally, speckle noise leads to the loss of important image details and reduces contrast. Mathematically, the speckle noise model is commonly represented as follows [1]:

$$\mathbf{f} = \mathbf{u} + \sqrt{\mathbf{u}}\boldsymbol{\eta}, \tag{1}$$

where, $\mathbf{f}$ denotes the observed image (the image affected by noise) of size $n \times n$, $\mathbf{u}$ represents the original image, and $\boldsymbol{\eta}$ is the noise component, which is approximated as Gaussian noise with zero mean and variance σ^2.

One of the main challenges in speckle noise filtering is to ensure the preservation of important image features, such as edges and textures, while achieving high efficiency in noise removal [2]. However, many existing denoising techniques often result in image blurring, leading to reduced resolution and loss of detail [3]. To overcome these limitations, numerous methods have been proposed with the aim of reducing speckle noise while maintaining image features [4, 5]. Among these, variational models based on Total Variation (TV) have attracted significant attention in the research community [1, 7-9]. The TV method is widely used as a regularization tool in speckle noise processing problems due to its outstanding ability to preserve sharp discontinuities and maintain edge structures during image restoration [10-15].

Based on model (1), Jin et al. proposed the following variational model for speckle noise removal [16]:

$$\min_{\mathbf{u}\in\Omega} \int_\Omega |\nabla \mathbf{u}|\, dx + \lambda \int_\Omega \frac{(\mathbf{f}-\mathbf{u})^2}{\mathbf{u}}\, dx, \tag{2}$$

where, $\Omega \subset \mathbb{R}^2$ is an open domain with a bounded boundary, $\int_\Omega |\nabla \mathbf{u}|$ denotes the first-order total variation of $\mathbf{u}$, λ is a positive parameter.

Huang et al. proposed an improvement to model (2) by introducing a convex variational model for speckle noise removal based on the Kullback-Leibler divergence, by substituting $\mathbf{z} = \log(\mathbf{u})$ [17], as follows (TV-Speckle model, TV-S):

$$\min_{\mathbf{z}\in\Omega} \int_\Omega |\nabla \mathbf{z}|\, dx + \lambda \int_\Omega \left(\mathbf{f}e^{-\frac{\mathbf{z}}{2}}\log\frac{\mathbf{f}}{e^{\mathbf{z}}} - \mathbf{f}e^{\frac{\mathbf{z}}{2}} + e^{\frac{\mathbf{z}}{2}}\right) dx \tag{3}$$

First-order total variation models, such as those in (2) and (3), have a notable drawback: the denoised results often exhibit the blocky effect and loss of fine details (staircasing phenomenon). To address this issue, several higher-order total variation models have been proposed, such as combining first- and second-order total variation [1], total generalized variation (TGV) [18], and its improvements [19, 20].

Second-order total generalized variation models for speckle noise removal allow for better noise suppression and outperform first-order variational methods by effectively reducing the staircasing effect. However, for images with pronounced directional textures, the challenge is not only to reduce noise and staircasing but also to preserve the directional characteristics of the image. Directional total generalized variation (DTGV) has been proposed to address this issue [19-22]. The high-order directional total generalized variation model (DTGV) is an extension of the original total generalized variation. The main improvement lies in the use of a directional weight, which is computed based on edge information within the image. Thanks to this weighting, DTGV can better process and preserve image details along prominent directions [20].

In this study, we incorporate directional total generalized variation (DTGV) into the existing data fidelity component to construct an objective function for speckle noise removal. The denoising method based on DTGV not only outperforms compared methods in edge preservation but also effectively eliminates the staircasing effect in the denoised images.

2. Related theories

Directional total generalized variation

The directional total generalized variation (DTGV) was proposed to capture the main direction in a noisy image while simultaneously preserving image details along the specified principal direction during the denoising process. The most common form is the second-order DTGV, which is expressed as follows [22]:

$$\mathrm{DTGV}^2(\mathbf{u}) = \min_{\mathbf{v}}\left(\lambda_1\left\|\tilde{\nabla}\mathbf{u} - \mathbf{v}\right\| + \lambda_0\|\tilde{\varepsilon}\mathbf{v}\|\right), \tag{4}$$

where $\mathbf{v} \in \mathrm{R}^{n\times n}$, $\tilde{\nabla} \in \mathbb{R}^{2n\times n}$ is the discrete gradient operator; $\tilde{\varepsilon}$ is the directional symmetric derivative operator of $\mathbf{v}$; and the parameters $\alpha_0, \alpha_1 \in (0, +\infty)$; $\nabla\mathbf{u} = \begin{bmatrix}\nabla_x^+\mathbf{u} \\ \nabla_y^+\mathbf{u}\end{bmatrix}$, where $\nabla_x^+\mathbf{u}$ and $\nabla_y^+\mathbf{u} \in \mathbb{R}^{n\times n}$ are the forward difference gradient operators:

$$(\nabla_x^+\mathbf{u})_{i,j} = \begin{cases} u_{i+1,j} - u_{i,j} \text{ if } 1 \le i < n, 1 \le j \le n, \\ 0 \text{ if } i = n \end{cases}$$

$$(\nabla_y^+\mathbf{u})_{i,j} = \begin{cases} u_{i,j+1} - u_{i,j} \text{ if } 1 \le i \le n, 1 \le j < n \\ 0 \text{ if } j = n \end{cases}$$

Similarly, $\nabla_x^-\mathbf{u}$ and $\nabla_y^-\mathbf{u} \in \mathbb{R}^{n\times n}$ are the backward difference gradient operators:

$$(\nabla_x^-\mathbf{u})_{i,j} = \begin{cases} u_{i,j} - u_{i-1,j} \text{ if } 1 \le i < n, 1 \le j \le n \\ 0 \text{ if } i = 0 \text{ or } i = n, 1 \le j \le n \end{cases}$$

$$(\nabla_y^-\mathbf{u})_{i,j} = \begin{cases} u_{i,j} - u_{i,j-1} \text{ if } 0 \le i \le n, 0 < j < n \\ 0 \text{ if } j = 0 \text{ or } j = n \end{cases}$$

The divergence operator is defined as $\mathrm{div} = -\nabla = (\nabla_x^-, \nabla_y^-)$. We define the rotation matrix R_θ and the scaling matrix $\mathcal{A}_a$ [22] as:

$$\mathrm{R}_\theta = \begin{bmatrix}\cos\theta & -\sin\theta \\ \sin\theta & \cos\theta\end{bmatrix}, \quad \mathcal{A}_a = \begin{bmatrix}1 & 0 \\ 0 & \alpha\end{bmatrix}$$

According to [20], we have: $\widetilde{\mathrm{div}}\,\mathbf{v} = \mathrm{div}\,\tilde{\mathbf{v}}$, with $\tilde{\mathbf{v}} = \mathcal{A}_a\mathrm{R}_{-\theta}\mathbf{v}$. Thus, by incorporating rotation and scaling into the difference method, we obtain the directional difference $\tilde{\nabla}\mathbf{u} = \mathcal{A}_a\mathrm{R}_{-\theta}\nabla\mathbf{u}$, and the directional symmetric derivative of $\mathbf{v}$ is calculated by [22, 23]:

$$(\tilde{\varepsilon}\mathbf{v})_{i,j} = \frac{1}{2}\left[\mathcal{A}_a\mathrm{R}_\theta\begin{bmatrix}(\nabla_x^-\mathbf{v}^1)_{i,j} & (\nabla_x^-\mathbf{v}^2)_{i,j} \\ (\nabla_y^-\mathbf{v}^1)_{i,j} & (\nabla_y^-\mathbf{v}^2)_{i,j}\end{bmatrix}\begin{bmatrix}(\nabla_x^-\mathbf{v}^1)_{i,j} & (\nabla_y^-\mathbf{v}^1)_{i,j} \\ (\nabla_x^-\mathbf{v}^2)_{i,j} & (\nabla_y^-\mathbf{v}^2)_{i,j}\end{bmatrix}\mathrm{R}_\theta^{\mathrm{T}}\mathcal{A}_a\right]$$

with $\widetilde{\mathrm{div}} = -\tilde{\varepsilon}$.

Equation (4) can thus be rewritten as:

$$\mathrm{DTGV}^2(\mathbf{u}) = \min_{\mathbf{v}}(\lambda_1\|\mathcal{A}_a\mathrm{R}_{-\theta}\nabla\mathbf{u} - \mathbf{v}\| + \lambda_0\|\tilde{\varepsilon}\mathbf{v}\|) \tag{5}$$

Edge detection function

In addition to preserving the main direction of the image, edge-preserving techniques also aim to retain significant boundaries during the denoising process. The edge-preserving function $\mathrm{g}(\mathbf{u})$ is defined as follows [23]:

$$\mathrm{g}(\mathbf{u}) = \frac{1}{1+\gamma|\nabla\mathcal{G}_\sigma * \mathbf{u}|^2} \tag{6}$$

where $\mathcal{G}_\sigma$ is a Gaussian filter with standard deviation σ_g, γ is a positive parameter. This function is designed to preserve edges while smoothing other regions of the image, thereby improving the overall image quality after denoising.

3. Proposed model

In this section, we propose a new model for removing speckle noise from digital images. The main objective of our approach is to combine DTGV (5) with the edge detection function (6), replacing $\tilde{\nabla}\mathbf{u} = \mathcal{A}_a\mathrm{R}_{-\theta}\mathrm{g}(\mathbf{u})$. Thus, the discrete form of second-order DTGV in (5) can be rewritten as follows [24]:

$$\mathrm{DTGV}^2(\mathbf{u}) = \lambda_1\|\mathcal{A}_a\mathrm{R}_\theta\mathrm{g}(\mathbf{u}) - \mathbf{v}\|_2 + \lambda_0\|\tilde{\varepsilon}\mathbf{v}\| \tag{7}$$

From (1), it can be seen that the noisy image is modeled as the original image plus the product of the original image and the noise component. Therefore, speckle noise is a special type of multiplicative noise, commonly encountered in measurement imaging applications, with pronounced noise characteristics that can significantly affect fine image details. In this study, we propose a data fidelity term for multiplicative noise removal [25], combined with the second-order DTGV method (7), to address the problem of speckle noise removal as follows (DTGV-g model):

$$\begin{aligned}\underset{\mathbf{u},\mathbf{v}}{\mathrm{argmin}} \int_\Omega \left(\frac{\mathbf{f}}{\sqrt{\mathbf{u}}}\log\frac{\mathbf{f}}{\mathbf{u}} - \frac{\mathbf{f}}{\sqrt{\mathbf{u}}} + \sqrt{\mathbf{u}} + \alpha\left(\sqrt{\frac{\mathbf{u}}{\mathbf{f}}} - 1\right)^2\right)\mathrm{dx} \\ +\lambda_1\|\mathcal{A}_a\mathrm{R}_\theta\mathrm{g}(\mathbf{u}) - \mathbf{v}\|_2 + \lambda_0\|\tilde{\varepsilon}\mathbf{v}\|\end{aligned} \tag{8}$$

In the case where a deblurring kernel $\mathbf{A}$ is present in the image in addition to noise, model (8) takes the

following form:

$$\underset{\mathbf{u},\mathbf{v}}{\operatorname{argmin}} \langle \frac{\mathbf{f}}{\sqrt{\mathbf{Au}}} \log \frac{\mathbf{f}}{\mathbf{Au}} - \frac{\mathbf{f}}{\sqrt{\mathbf{Au}}} + \sqrt{\mathbf{Au}} + \alpha \left(\sqrt{\frac{\mathbf{Au}}{\mathbf{f}}} - 1 \right)^2, \mathbf{1} \rangle + \lambda_1 \| \mathcal{A}_a R_\theta g(\mathbf{u}) - \mathbf{v} \|_2 + \lambda_0 \| \tilde{\varepsilon} \mathbf{v} \| \quad (9)$$

There are several methods to solve problem (9). In this paper, we use the Chambolle–Pock algorithm [26] to optimize (8), and rewrite it in its dual form as follows:

$$\underset{\mathbf{u},\mathbf{v}}{\operatorname{argmin}} \underset{\mathbf{q},\mathbf{p},\mathbf{w}}{\operatorname{argmax}} \langle \frac{\mathbf{f}}{\sqrt{\mathbf{Au}}} \log \frac{\mathbf{f}}{\mathbf{Au}} - \frac{\mathbf{f}}{\sqrt{\mathbf{Au}}} + \sqrt{\mathbf{Au}} + \alpha \left(\sqrt{\frac{\mathbf{Au}}{\mathbf{f}}} - 1 \right)^2, \mathbf{q} \rangle + \lambda_1 \langle \mathcal{A}_a R_\theta g(\mathbf{u}) - \mathbf{v}, \mathbf{p} \rangle + \lambda_0 \langle \tilde{\varepsilon} \mathbf{v}, \mathbf{w} \rangle \quad (10)$$

where $\mathbf{p}, \mathbf{q}, \mathbf{w}$ are the dual variables.

To solve problem (10), we initialize the variables as $\mathbf{p} = 0, \mathbf{q} = 0, \mathbf{w} = \mathbf{0}, \mathbf{u} = \tilde{\mathbf{u}} = \mathbf{f}, \mathbf{v} = \tilde{\mathbf{v}} = 0$. Additionally, we need to estimate the deblurring kernel $\mathbf{A}$ and auxiliary parameters $\tau > 0$ and $\eta > 0$. The algorithm iterates through the following steps:

$$\mathbf{p}^{k+1} = \underset{\mathbf{p}}{\operatorname{argmax}} \lambda_1 \langle \Lambda_a R_{-\theta} g(\mathbf{A}\bar{\mathbf{u}}^k) - \bar{\mathbf{v}}^k, \mathbf{p} \rangle - \frac{1}{2\eta}, \quad (11)$$

$$\mathbf{w}^{k+1} = \underset{\mathbf{w}}{\operatorname{argmax}} \lambda_0 \langle \tilde{\mathcal{E}} \bar{\mathbf{v}}^k, \mathbf{w} \rangle - \frac{1}{2\eta} \| \mathbf{w} - \mathbf{w}^k \|_2^2, \quad (12)$$

$$\mathbf{q}^{k+1} = \underset{\mathbf{q}}{\operatorname{argmax}} \left\langle \frac{\mathbf{f}}{\sqrt{\mathbf{A}\bar{\mathbf{u}}^k}} \log \frac{\mathbf{f}}{\mathbf{A}\bar{\mathbf{u}}^k} - \frac{\mathbf{f}}{\sqrt{\mathbf{A}\bar{\mathbf{u}}^k}} + \sqrt{\mathbf{A}\bar{\mathbf{u}}^k} + \alpha \left(\sqrt{\frac{\mathbf{A}\bar{\mathbf{u}}^k}{\mathbf{f}}} - 1 \right)^2, \mathbf{q} \right\rangle - \frac{1}{2\eta} \left\| \mathbf{q} - \mathbf{q}^k \right\|_2^2, \quad (13)$$

$$\mathbf{u}^{k+1} = \underset{\mathbf{Au}}{\operatorname{argmin}} \left\langle \frac{\mathbf{f}}{\sqrt{\mathbf{Au}}} \log \frac{\mathbf{f}}{\mathbf{Au}} - \frac{\mathbf{f}}{\sqrt{\mathbf{Au}}} + \alpha \left(\sqrt{\frac{\mathbf{Au}}{\mathbf{f}}} - 1 \right)^2, \mathbf{q} \right\rangle + \langle \mathcal{A}_a R_{-\theta} g(\mathbf{Au}), \mathbf{p} \rangle + \frac{1}{2\tau} \| \mathbf{Au} - \mathbf{Au}^k \|_2^2, \quad (14)$$

$$\mathbf{v}^{k+1} = \underset{\mathbf{v}}{\operatorname{argmin}} - \langle \mathbf{v}, \mathbf{p}^{k+1} \rangle + \langle \tilde{\mathcal{E}} \bar{\mathbf{v}}^k, \mathbf{w} \rangle + \frac{1}{2\tau} \| \mathbf{v} - \mathbf{v}^k \|_2^2. \quad (15)$$

The dual variables $\mathbf{p}, \mathbf{w}, \mathbf{q}$ ở (11), (12), (13) are updated using set-projection [26], defined as follows:

$$[\mathcal{S}_\lambda(\mathbf{x})]_{i,j} = \frac{\mathbf{x}_{i,j}}{\max\left(1, \frac{\mathbf{x}_{i,j}}{\lambda}\right)}$$

Thus, the updates for $\mathbf{p}, \mathbf{q}, \mathbf{w}$ are:

$$\mathbf{p}^{k+1} = \mathcal{S}_{\lambda_1} \left(\mathbf{p}^k + \eta \left(\mathcal{A}_a R_{-\theta} g(\mathbf{A}\bar{\mathbf{u}}^k) - \bar{\mathbf{v}}^k \right) \right)$$

$$\mathbf{q}^{k+1} = \mathcal{S}_1 \left(\mathbf{q}^k + \eta \left(\frac{\mathbf{f}}{\sqrt{\mathbf{A}\bar{\mathbf{u}}^k}} \log \frac{\mathbf{f}}{\mathbf{A}\bar{\mathbf{u}}^k} - \frac{\mathbf{f}}{\sqrt{\mathbf{A}\bar{\mathbf{u}}^k}} + \sqrt{\mathbf{A}\bar{\mathbf{u}}^k} + \alpha \left(\sqrt{\frac{\mathbf{A}\bar{\mathbf{u}}^k}{\mathbf{f}}} - 1 \right)^2 \right) \right)$$

$$\mathbf{w}^{k+1} = \mathcal{S}_{\lambda_0} \left(\mathbf{w}^k + \eta \tilde{\mathcal{E}} \bar{\mathbf{v}}^k \right)$$

Using the gradient descent method, we update the value $\mathbf{u}^{k+1}$ in (14) as follows:

$$\mathbf{u}^{k+1} = \mathbf{Au}^k + \tau \left(\widetilde{\operatorname{div}} \mathbf{p}^{k+1} - \left(\frac{\mathbf{f}}{2\mathbf{Au}\sqrt{\mathbf{Au}}} \left(\log \frac{\mathbf{Au}}{\mathbf{f}} - 1 \right) + \frac{1}{2\sqrt{\mathbf{Au}}} + \frac{\alpha}{\mathbf{f}} - \frac{\alpha}{\sqrt{\mathbf{Auf}}} \right) \mathbf{q}^{k+1} \right)$$

For the subproblem in $\mathbf{v}$ (15), we have:

$$\mathbf{v}^{k+1} = \mathbf{v}^k + \tau \left(\widetilde{\operatorname{div}} \mathbf{w}^{k+1} + \mathbf{p}^{k+1} \right)$$

Finally, we update the variables $\bar{\mathbf{u}}$ and $\bar{\mathbf{v}}$ as follows:

$$\bar{\mathbf{u}}^{k+1} = 2\mathbf{u}^{k+1} - \mathbf{u}^k$$
$$\bar{\mathbf{v}}^{k+1} = 2\mathbf{v}^{k+1} - \mathbf{v}^k$$

The stopping criterion for the iteration can be based on the convergence of the objective function or the change in the main variable $\mathbf{u}$.

4. Experiments

In this section, simulations are conducted to verify the effectiveness of the proposed model, using standard grayscale images[1] of size 256×256, as shown in Figure 1: (a) Boat, (b) Man, (c) Couple, (d) Crowd, (e) Lake, (f) Pepper, (g) Car, (h) Zelda. The experiments were carried out in MATLAB R2023b on a system with an Intel Core i5-12600KF CPU and 16GB RAM. The experiments include denoising, as well as simultaneous denoising and deblurring. The observed images were generated using MATLAB. The Peak Signal-to-Noise Ratio (PSNR) and Structural Similarity Index (SSIM) metrics were used to evaluate the quality of the restored images compared to the original images [27]. The results were then compared with four other methods: TV-S [17], DTGV [20], TV-L1 [26], and Anisotropic Diffusion Filter (ADF) [28].

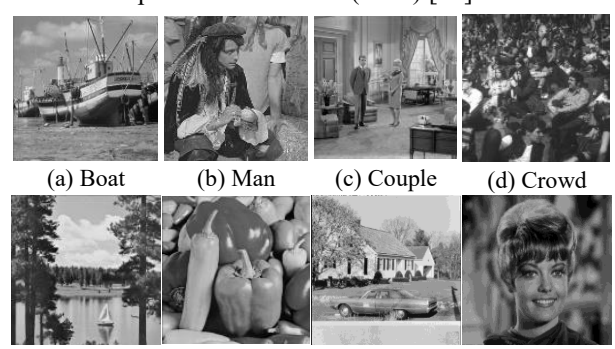

(a) Boat (b) Man (c) Couple (d) Crowd

(e) Lake (f) Pepper (g) Car (h) Zelda

Figure 1. *Images used in the experiments*

- Image denoising experiment: In this case, the proposed model is represented by equation (8). Figure 2 visually displays the denoising results of the compared methods at a noise level of $\sigma = 2$, while Figure 4 shows the results at a noise level of $\sigma = 3$. The denoised results with zoomed-in details are presented in Figures 3 and 5, respectively.

From the result images, our DTGV-g model not only achieves effective noise removal but also simultaneously preserves image edges. The performance of the models is

[1] http://www.dip.ee.uct.ac.za/imageproc/stdimages/greyscale/

measured using the PSNR and SSIM metrics, which are presented in Tables 1 and 2. In the case of $\sigma = 2$, our model significantly outperforms the other models in both PSNR and SSIM. Furthermore, in the case of a higher noise level $\sigma = 3$, our model still yields better results than the other models in most cases.

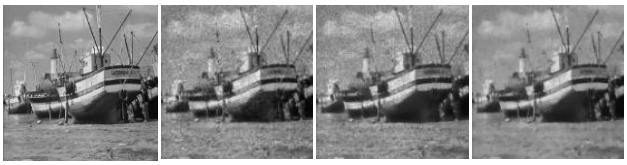

(a) Original (b) Noisy (c) ADF (d) TV-L1

(e) DTGV (f) TV-S (g) DTGV-g

Figure 2. *Denoising results with noise level σ=2*

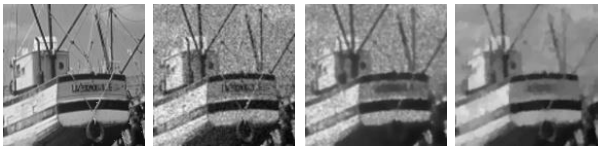

(a) Original (b) Noisy (c) ADF (d) TV-L1

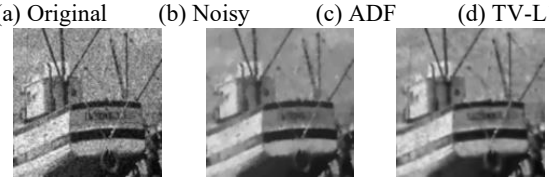

(e) DTGV (f) TV-S (g) DTGV-g

Figure 3. *Enlarged detail of the result in Figure 2*

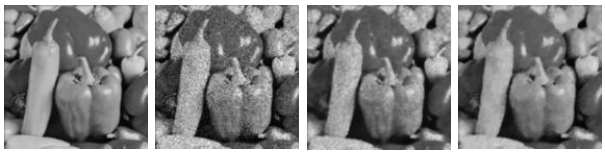

(a) Original (b) Noisy (c) ADF (d) TV-L1

(e) DTGV (f) TV-S (g) DTGV-g

Figure 4. *Denoising results with noise level $\sigma = 3$*

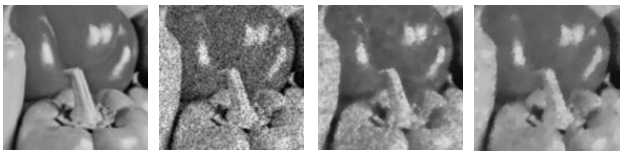

(a) Original (b) Noisy (c) ADF (d) TV-L1

(e) DTGV (f) TV-S (g) DTGV-g

Figure 5. *Enlarged detail of the result in Figure 4*

- Image deblurring and denoising experiment: In this case, the proposed model is represented by equation (9). In practice, image noise is often accompanied by blurring, which further degrades the overall image quality. This section simulates images affected simultaneously by both noise and blur and compares the effectiveness of the models in handling joint denoising and deblurring. To conduct the simulation, we apply a blurring operator using a Gaussian filter with K sizes of 3×3 and 5×5, a standard deviation of 2, followed by the addition of speckle noise with $\sigma = 2$.

Table 1. *PSNR results of different methods at various noise levels*

Images	σ	Noisy	ADF	TV-L1	DTGV	TV-S	DTGV-g
Boat	2	21.0119	23.7021	24.9313	21.1353	26.3577	**26.8617**
	3	17.4901	22.6131	24.009	17.6597	24.8511	**24.9763**
Man	2	21.1637	23.602	23.5073	21.749	24.811	**25.6722**
	3	17.6419	22.9779	22.7574	18.2914	23.6536	**23.7060**
Couple	2	21.6297	25.6037	26.7498	21.6997	27.3686	**28.2719**
	3	18.1079	23.4992	25.4169	19.0712	25.9026	**26.2597**
Crowd	2	19.4395	26.1889	26.5039	23.0409	27.3037	**28.2825**
	3	15.9177	24.6063	24.9434	18.5841	26.1541	**26.2306**
Lake	2	21.1937	23.6295	26.3877	21.4415	27.0537	**27.5079**
	3	17.6718	23.3885	24.8233	18.1285	25.386	**25.6327**
Peppers	2	21.0733	26.2167	28.9501	21.4329	29.5063	**29.8638**
	3	17.5515	24.9367	27.0961	18.0198	27.3239	**27.3692**
Car	2	21.1981	22.0720	24.6652	21.5105	25.5105	**25.8945**
	3	19.2762	21.0422	23.6314	19.4773	23.8928	**24.1823**
Zelda	2	25.3362	29.3112	30.0302	25.6237	30.7124	**31.4602**
	3	21.8143	27.2039	28.4354	22.0965	29.1023	**29.4646**

Table 2. *SSIM results of different methods at various noise levels*

Images	σ	Noisy	ADF	TV-L1	DTGV	TV-S	DTGV-g
Boat	2	0.4745	0.5823	0.6810	0.4788	0.7318	**0.7555**
	3	0.3400	0.5372	0.6309	0.3460	0.6495	**0.6564**
Man	2	0.2767	0.6417	0.6333	0.5889	0.6839	**0.7438**
	3	0.1805	0.6117	0.5845	0.4415	0.6289	**0.6373**
Couple	2	0.5851	0.6754	0.7327	0.5909	0.7509	**0.7929**
	3	0.4367	0.5732	0.6693	0.4487	0.6824	**0.6981**
Crowd	2	0.2891	0.8027	0.8087	0.5967	0.8259	**0.8718**
	3	0.2063	0.7246	0.7495	0.4378	0.7992	**0.8060**
Lake	2	0.5354	0.5845	0.8025	0.5380	0.8051	**0.8203**
	3	0.4012	0.5975	0.7311	0.4225	0.7278	**0.7331**
Peppers	2	0.4582	0.7556	0.8472	0.4615	0.8679	**0.8822**
	3	0.2993	0.6878	0.8056	0.3041	0.8085	**0.8157**
Car	2	0.5898	0.5310	0.6978	0.5127	0.7257	**0.7407**
	3	0.4304	0.4631	0.6444	0.4384	0.6141	**0.6280**
Zelda	2	0.4769	0.8060	0.8275	0.4857	0.8482	**0.8778**
	3	0.3182	0.7150	0.7795	0.3881	0.8030	**0.8279**

The results of deblurring and denoising are shown in Figure 6 (for a 3×3 blur kernel), Figure 8 (for a 5×5 blur kernel). Similarly, the zoomed-in details of the resulting images are illustrated in Figures 7 and 9. The PSNR and SSIM results for the deblurred and denoised images are summarized in Tables 3 and 4.

(a) Original (b) Noisy (c) ADF (d) TV-L1

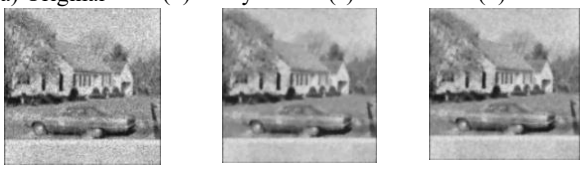

(e) DTGV (f) TV-S (g) DTGV-g

Figure 6. *Denoising and deblurring results with K=3*

Table 3. *Comparison of PSNR results for simultaneous deblurring and denoising*

Images	*K*	Noisy	ADF	TV-L1	DTGV	TV-S	DTGV-g
Boat	3	19.7533	22.9932	23.4525	19.8372	23.7239	**23.9108**
	5	19.1136	22.1008	22.3924	19.1822	22.5718	**22.6687**
Man	3	19.4975	21.8862	21.8848	19.5598	22.0922	**22.2028**
	5	18.7455	20.7904	20.9551	18.7975	21.0841	**21.1768**
Couple	3	20.4808	24.4644	24.5322	20.5718	25.2023	**25.4891**
	5	19.8142	23.4009	23.6369	19.8902	23.8223	**23.9250**
Crowd	3	21.9104	24.0911	24.5322	22.0765	25.0544	**25.0938**
	5	20.9198	23.0224	23.1096	21.0377	23.4359	**23.6018**
Lake	3	20.4471	22.5347	24.3230	22.6422	24.5687	**24.6235**
	5	19.5984	21.7670	22.7809	19.7515	22.9627	**23.0884**
Peppers	3	20.8740	25.3269	26.8049	21.9601	27.0164	**27.1193**
	5	20.3183	24.0631	25.0099	20.3902	25.3290	**25.8001**
Car	3	18.8761	21.2398	22.7763	19.0280	22.9151	**23.0891**
	5	18.2471	20.5047	21.6058	18.3705	21.6931	**21.7202**
Zelda	3	22.1569	28.5234	28.6603	22.2469	29.1735	**29.2736**
	5	21.8508	27.6297	27.5111	21.9404	27.9834	**30.7584**

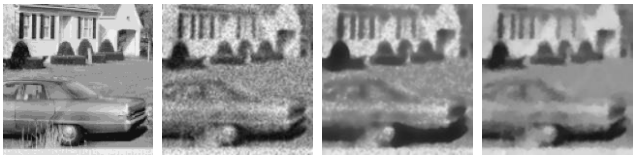

(a) Original (b) Noisy (c) ADF (d) TV-L1

(e) DTGV (f) TV-S (g) DTGV-g

Figure 7. *Enlarged detail of the result in Figure 6*

(a) Original (b) Noisy (c) ADF (d) TV-L1

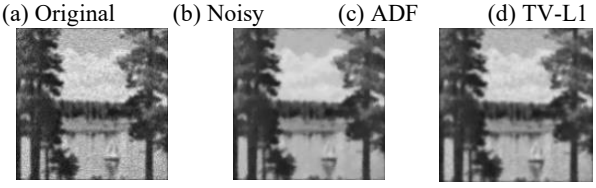

(e) DTGV (f) TV-S (g) DTGV-g

Figure 8. *Denoising and deblurring results with K=5*

Table 4. *Comparison of SSIM results for simultaneous deblurring and denoising*

Images	*K*	Noisy	ADF	TV-L1	DTGV	TV-S	DTGV-g
Boat	3	0.3401	0.5692	0.6084	0.3447	0.6260	**0.6276**
	5	0.2689	0.5217	0.5527	0.2730	0.5488	**0.5528**
Man	3	0.3737	0.5014	0.5335	0.3772	0.5419	**0.5597**
	5	0.2839	0.4391	0.4688	0.2866	0.4749	**0.4827**
Couple	3	0.3733	0.6258	0.7375	0.3769	0.6689	**0.6806**
	5	0.2951	0.5727	0.6881	0.2983	0.6009	**0.6084**
Crowd	3	0.5162	0.7124	0.7375	0.5224	0.7532	**0.7722**
	5	0.4346	0.6627	0.6681	0.4402	0.6830	**0.7037**
Lake	3	0.4323	0.5439	0.7170	0.4425	0.8331	**0.7995**
	5	0.3562	0.5216	0.6905	0.3602	0.7688	**0.7882**
Peppers	3	0.3791	0.7157	0.7170	0.3825	0.7998	**0.8067**
	5	0.3413	0.6905	0.6905	0.3445	0.7824	**0.7882**
Car	3	0.3167	0.4627	0.5912	0.3210	0.5987	**0.6108**
	5	0.2511	0.4134	0.5493	0.2548	0.5480	**0.5561**
Zelda	3	0.3880	0.7954	0.7990	0.3933	0.8183	**0.8398**
	5	0.3540	0.7758	0.7683	0.3594	0.7905	**0.8649**

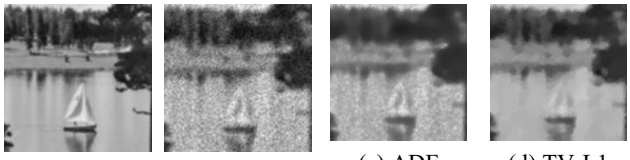

(a) Original (b) Noisy (c) ADF (d) TV-L1

(e) DTGV (f) TV-S (g) DTGV-g

Figure 9. *Enlarged detail of the result in Figure 8*

From the experimental results, it can be seen that the proposed method demonstrates competitive performance compared to the other methods. Even in cases where the images are simultaneously blurred and noisy, the proposed solution still performs well relative to the compared methods. The zoomed-in details of the restored images show that edges and image attributes are preserved more clearly than with the other methods. This confirms the effectiveness of the proposed method in speckle noise removal and its ability to improve image quality.

5. Conclusion

In this study, we proposed a novel speckle noise removal model based on DTGV combined with an edge detection method. This approach enables effective noise removal while preserving important image features, including edges and textures. By employing the Chambolle-Pock algorithm, the method achieves high performance in both processing speed and output image quality. Experimental results on various image datasets demonstrate that our method outperforms the compared methods. Notably, in cases of severe speckle noise or blurring, the DTGV-g model is still able to restore images with high quality, maintaining better detail compared to the other methods. This confirms that our method has great potential for widespread application in fields such as medical image processing, computer vision, and satellite image analysis.

REFERENCES

[1] S. Wang, T. Z. Huang, X. L. Zhao, J.J. Mei and J. Huang, "Speckle noise removal in ultrasound images by first- and second-order total variation", *Numer. Algorithms*, vol. 78, pp. 513–533, 2018. https://doi.org/10.1007/s11075-017-0386-x

[2] L. Fan, F. Zhang, H. Fan, and C. Zhang, "Brief review of image denoising techniques, *Vis. Comput. Ind. Biomed. Art*, vol. 2, no. 7, pp. 1-12, 2019. https://doi.org/10.1186/s42492-019-0016-7

[3] A. Misra, B. Kartikeyan and S. Garg, "Wavelet based SAR data denoising and analysis", *in Proc. IEEE Int. Adv. Comput. Conf.,* Gurgaon, India, 2014, pp. 1087-1092.

[4] P.N. Devi and R. Asokan, "An improved adaptive wavelet shrinkage for ultrasound", *Sadhana*, vol. 39, pp. 971–988, 2014. https://doi.org/10.1007/s12046-014-0254-5

[5] S. Pradeep and P. Nirmaladevi, "A Review on Speckle Noise Reduction Techniques in Ultrasound Medical images based on Spatial Domain, Transform Domain and CNN Methods", *IOP Conf. Ser.: Mater. Sci. Eng.*, 1055, 012116, pp. 1-9, 2021. https://doi.org/10.1088/1757-899X/1055/1/012116

[6] K. Sikhakhane, S. Rimer, M. Gololo, K. Ouahada and A. M. Abu-Mahfouz, "Evaluation of Speckle Noise Reduction Filters and Machine Learning Algorithms for Ultrasound Images", *IEEE Access*, vol. 12, pp. 81293-81312, 2024. https://doi.org/10.1109/ACCESS.2024.3411709

[7] R. Ren, Z. Guo, Z. Jia, J. Yang, N. K. Kasabov and C. Li, "Speckle Noise Removal in Image-based Detection of Refractive Index Changes in Porous Silicon Microarrays", *Sci. Rep.*, vol. 9, 15001 pp. 1-14, 2019. https://doi.org/10.1038/s41598-019-51435-y

[8] S. V. Parhad, S. A. Aher and K. K. Warhade, "A Comparative Analysis of Speckle Noise Removal in SAR Images", *Proc. 2nd Glob. Conf. Adv. Technol.*, Bangalore, India, 2021, pp. 1-4. https://doi.org/10.1109/GCAT52182.2021.9587458.

[9] G. Gong, H. Zhang and M. Yao, "Speckle noise reduction algorithm with total variation regularization in optical coherence tomography", *Opt. Express*, vol. 23, pp. 24699-24712, 2015. https://doi.org/10.1364/OE.23.024699

[10] S. K. Panigrahi, "Speckle Noise Removal by Total Variation and Curvelet Coefficient Shrinkage of Residual Noise", *in Proc. Int. Conf. Wirel. Commun. Signal Process. Netw.,* Chennai, India, 2019, pp. 101-106.

[11] A. B. Misra, E. Lockhart, and H. Lim, "Total variation based denoising methods for speckle noise images", *Involve*, vol. 10, no. 2, pp. 327-344, 2017. https://doi.org/0.2140/involve.2017.10.327

[12] L. Wang, L. Xiao, L. Huang and Z. Wei, "Nonlocal total variation based speckle noise removal method for ultrasound image", *in Proc. 4th Int. Congr. Image Signal Process.*, Shanghai, China, 2011, pp. 709-713.

[13] B. Chen, J. Zou, W. Chen, X. Kong, J. Ma and F. Li, "Speckle Noise Removal Based on Adaptive Total Variation Model", *In Proc. Pattern Recognit. Comput. Vis.,* Guangzhou, China, 2018, pp. 191–202.

[14] S. Cuomo, M. D. Rosa, S. Izzo, F. Piccialli, and M. Pragliola, "Speckle noise removal via learned variational models", *Appl. Numer. Math.*, vol. 200, pp. 162-178, 2024. https://doi.org/10.1016/j.apnum.2023.06.002

[15] N. Rawat, M. Singh, and B. Singh, "Wavelet and Total Variation Based Method Using Adaptive Regularization for Speckle Noise Reduction in Ultrasound Images", *Wirel. Pers. Commun.*, vol. 106, pp. 1547-1572, 2019. https://doi.org/10.1007/s11277-019-06229-w

[16] Z. Jin and X. Yang, "A variational model to remove the multiplicative noise in ultrasound images", *J. Math. Imaging Vis.*, vol. 39, pp. 62-74, 2010. https://doi.org/10.1007/s10851-010-0225-3

[17] J. Huang and X. Yang, "Fast reduction of speckle noise in real ultrasound images", *Signal Process.*, vol. 93, no. 4, pp. 684-694, 2013. https://doi.org/10.1016/j.sigpro.2012.09.005

[18] K. Bredies, K. Kunisch, and T. Pock, "Total generalized variation," *SIAM J. Imaging Sci.*, vol. 3, no. 3, pp. 492-526, 2010. https://doi.org/10.1137/090769521

[19] D. Serafino, G. Landi, and M. Viola, "Directional TGV-based image restoration under poisson noise," *J. Imaging*, vol. 7, no. 6, pp. 1-18, 2021. https://doi.org/10.3390/jimaging7060099

[20] R. D. Kongskov, Y. Dong, and K. Knudsen, "Directional total generalized variation regularization", *BIT Numer. Math.*, vol. 59, pp. 903-928, 2019. https://doi.org/10.1007/s10543-019-00755-6

[21] I. Bayram and M. E. Kamasak, "Directional Total Variation", *IEEE Signal Process. Lett.*, vol. 19, no. 12, pp. 781-784, 2012. https://doi.org/10.1109/LSP.2012.2220349

[22] R. D. Kongskov and Y. Dong, "Directional total generalized variation regularization for impulse noise removal", *in Proc. Scale Space Var. Methods Comput. Vis.*, Kolding, Denmark, 2017, pp. 221-231. https://doi.org/10.1007/978-3-319-58771-4_18

[23] X. Liu, "Weighted total generalised variation scheme for image restoration", *IET Image Process.*, vol. 10, no. 1, pp. 80-88, 2016. https://doi.org/10.1049/iet-ipr.2015.0013

[24] P.C. Thang, T.T. Cuong, N. N. Anh. Nguyen, and T. V. Hieu, "An Oriented High-Order Total Variation-Based Method for Multiplicative Noise Removal in Digital Images and Edge Enhancement" *in. Proc. XXVII Nat. Conf. Sel. Issues Inf. Commun. Technol.*, Nha Trang, Vietnam, 2024, pp. 392-397.

[25] Y. Dong and T. Zeng, "A Convex Variational Model for Restoring Blurred Images with Multiplicative Noise", *SIAM J. Imaging Sci.*, vol. 6, no. 3, pp. 1598-1625, 2013. https://doi.org/10.1137/120870621

[26] A. Chambolle and T. Pock, "A First-Order Primal-Dual Algorithm for Convex Problems with Applications to Imaging", *J. Math. Imaging Vis.*, vol. 40, pp. 120-145, 2011. https://doi.org/10.1007/s10851-010-0251-1

[27] Z. Wang and A.C. Bovik, *Modern Image Quality Assessment: Synthesis Lectures on Image, Video, and Multimedia Processing*, Morgan and Claypool Publishers, 2006.

[28] G. Ramos-Llorden, G. Vegas-Sanchez-Ferrero, M. Martin-Fernandez, C. Alberola-Lopez, and S. Aja-Fernandez, "Anisotropic diffusion filter with memory based on speckle statistics for ultrasound images", *IEEE Trans. Image Process.*, vol. 24, no. 1, pp. 345-358, 2014. https://doi.org/10.1109/tip.2014.237124